Mechanistic approach to enhancement of the yield of a sonochemical reaction

ARTICLE *in* AICHE JOURNAL · MAY 2007

Impact Factor: 2.75 · DOI: 10.1002/aic.11170

Mechanistic Approach to Enhancement of the Yield of a Sonochemical Reaction

Thirugnanasambandam Sivasankar, Ashwin W. Paunikar, and Vijayanand S. Moholkar
Dept. of Chemical Engineering, Indian Institute of Technology Guwahati, Guwahati 781039, Assam, India

DOI 10.1002/aic.11170
Published online March 26, 2007 in Wiley InterScience (www.interscience.wiley.com).

In this study, a mechanistic approach has been taken to enhance yield of a sonochemical reaction. Formation of highly reactive free radicals due to the transient collapse of cavitation bubbles is the primary mechanism of a sonochemical reaction. A physical (reduction in dissolved gas concentration) and a chemical (increasing the reactant concentration) technique is used for enhancing yield of a sonochemical reaction using those techniques, which influence the phenomenon of radical formation by the cavitation bubbles. A bubble dynamics model is used for explaining the sonochemical phenomena. In a degassed medium, the ultrasound wave undergoes lesser attenuation; moreover, equilibrium size of a bubble shrinks due to rectified diffusion. Because of this, a bubble undergoes more violent collapse, resulting in greater production of radicals that give higher yield. On the other hand, increasing the initial reactant concentration shows an adverse effect on the sonochemical yield. This is ascribed to reduction in water vapor flux in the bubble due to reduction of vapor pressure of the medium. This study, therefore, demonstrates as how macroscopic manifestation (the sonochemical yield) of the microscopic phenomena (transient collapse of cavitation bubble) is a complicated function of several physical processes. The results of this study shed light on the complex and multifaceted physical mechanism of a sonochemical reaction, which may be useful in maximization of yield of other sonochemical systems. © 2007 American Institute of Chemical Engineers *AIChE J,* 53: 1132–1143, 2007
Keywords: cavitation, bubble dynamics, sonochemistry

Introduction

The effect of ultrasound in enhancing the kinetics of several chemical reactions is well known.[1–3] This effect is attributed to the generation of highly reactive free radicals such as $O^{\cdot}$, $OH^{\cdot}$, $HO_2^{\cdot}$ due to the transient cavitation bubble collapse driven by the ultrasound wave. Ultrasound passes through the liquid medium in the form of a longitudinal wave comprising of alternate compression and rarefaction cycles, as a result of which the local pressure varies. This variation in local pressure brings about intense volume oscillations of existing cavitation nuclei (or free gas content) in the medium. The cavitation nuclei are tiny, free-floating bubbles in the liquid, or gas pockets trapped in the crevices of the solid boundaries in the liquid medium. Evaporation occurs at the gas–liquid interface with diffusion of vapor into the cavitation bubble. During the subsequent compression phase, the liquid vapor tends to condense at the bubble wall. An interesting phenomenon occurs at this time. During the final moments of collapse, the bubble wall velocity reaches or even exceeds the velocity of sound in water, and not all the vapor that has entered the bubble can escape. This vapor, thus, gets entrapped in the cavitation bubble. Extremes of temperature and pressure are reached in the bubble during instance of maximum compression (~5000 K and 500 bar) and the trapped vapor decomposes at these conditions into various radicals. These radicals get mixed with the bulk liquid with fragmentation of the bubble during collapse and

Correspondence concerning this article should be addressed to V. S. Moholkar at vmoholkar@iitg.ac.in.

induce chemical reaction or acceleration of the chemical reaction. The extent of radical formation in a single cavitation bubble is a function of two parameters: amount of water vapor trapped in the bubble and the temperature and pressure peak reached in the bubble during the transient collapse.

The rate of a chemical reaction induced by ultrasound: M + $R^{\bullet} \rightarrow$ products, can be represented as: Rate = k_R [M] [$R^{\bullet}$]; where [M] is the concentration of the reactant, [$R^{\bullet}$] is the concentration of the radicals resulting out of cavitation bubbles and k_R is the rate constant. The rate of the sonochemical reaction and the yield obtained during a specific reaction time can be enhanced by increasing either the initial reactant concentration or by increasing the radical production from the bubble. Another factor which influences the yield of the sonochemical reaction is the probability of interaction between a reactant molecule and the radicals produced out of bubble collapse. However, the radical production is confined in the medium only at the locations of cavitation events—not uniformly throughout the bulk medium. If the concentration of reactant molecules in the vicinity of a cavitation bubble is low, the radicals may recombine without undergoing any chemical change. The aim of the present study is to assess the effect of a physical (lowering the dissolved gas content or degassing of the liquid medium) and chemical (increasing the initial reactant concentration) technique on the enhancement of the yield of a sonochemical reaction. The chemical technique that we adopt follows directly from the rate expression given above, while the physical technique of degassing the liquid medium is in spirit of earlier works[4,5] of one of the authors of the present paper. In these works, it was demonstrated that reduction in the dissolved gas content of the medium, while maintaining the free gas content (or cavitation nuclei population) fairly constant, significantly enhances the cavitation intensity, and hence, the efficiency of the sonochemical reactor. As the sonochemical reaction is the chemical manifestation of cavitation phenomena, degassing of the medium is also likely to enhance the yield of such a reaction. Both of the techniques mentioned above influence the phenomenon of radical formation by cavitation bubbles (as we demonstrate in the subsequent sections), which the primary mechanism of a sonochemical reaction. Thus, this study addresses the matter of sonochemical yield from mechanistic point of view. For our study we choose a well-known chemical reaction induced by ultrasound: oxidation of potassium iodide (KI) to liberate iodine. For explaining the physical phenomena, we use a bubble dynamics model, which takes into account the heat diffusion and water vapor transport through the bubble during radial motion driven by ultrasound.

Several authors have dealt with the matter of sonochemical yield using KI oxidation as a model reaction[6–14] before. However, in these studies no attempt was made to explain the trends in iodine liberation using a bubble dynamics model. Few authors have tried to explain the variation in iodine liberation with different reaction conditions using a bubble dynamics model. Gogate et al.[15,16] have correlated the iodine liberation rate to the extremes of temperature and pressure obtained at the transient collapse using a bubble dynamics model. However, the model used by Gogate et al.[15,16] does not take into account the transport of water vapor and the entrapment of water vapor. Naidu et al.[17] explained the trends in the rate of iodine liberation with the sonication of aqueous KI solutions of various concentrations and under different gas atmospheres using Rayleigh-Plesset equation for the radial bubble motion coupled with Flynn's assumption[18] that the bubble becomes a closed system during collapse phase, when the partial pressure of gas becomes equal to the vapor pressure of water. Thus, the amount of water vapor in the bubble was kept same in all simulations, without modeling the continuous transport of water vapor during radial bubble motion. Moreover, the Rayleigh-Plesset equation does not take into account the compressibility of the liquid medium, and hence, Naidu et al.[17] terminated their simulations at the instance when the bubble wall velocity reaches the velocity of sound in water.

The present work addresses the matter of enhancement of the sonochemical yield with a different and more rigorous perspective. We take mechanistic approach of correlating the sonochemical yield to the fundamental phenomena of water vapor entrapment in cavitation bubbles resulting in generation of radicals, which is at the very basis of sonochemical reaction. The bubble dynamics model used in this study relaxes several assumptions made by earlier authors, which gives a more detailed description of the physics and chemistry of cavitation bubbles and its correlation with the sonochemical phenomena observed in the bulk medium. Therefore, in addition to the revelation of the efficacy of different techniques in enhancing the sonochemical yield, the results of the present study also provide an insight into the mechanism of the sonochemical phenomena and the complex nature of interactions between various physical parameters.

Experimental

Experimental setup

A schematic diagram of the experimental setup used in the present study is shown in Figure 1A. The experiments were done in a jacketed glass reactor (dimensions: height, 120 mm; diameter, 50 mm; inner jacket diameter, 62 mm). For bubbling of air during sonication (purpose of which is discussed later in this section), a gas sparger (or aerator) made of glass was used, the schematic of which is shown in Figure 1B along with relevant dimensions. In order to disperse the gas in the solution in the form of fine bubbles, the aerator had porous silica filter (pore size ~40 μm). During reactions, the aerator was so positioned that the porous silica filter exactly faces the bottom of the ultrasound tip. This ensured uniform distribution of the bubbles forming cavitation nuclei in the solution. The air flow rate through the sparger was set at 5 l/h using a rotameter. In order to maintain the bulk temperature constant during sonication, cooling water was circulated through the jacket of the reactor. For the sonication of KI solution, a microprocessor based and programmable ultrasound processor was used (Sonics and Materials, Model VCX 500). This processor had a frequency of 20 kHz with maximum power output of 500 W. The processor had variable power output control, which was set at 20% during experiments, resulting in consumption of 100 W power during sonication. It needs to be mentioned that this value corresponds to the theoretical maximum ultrasound intensity. The actual ultrasonic intensity in the medium was calibrated using calorime-

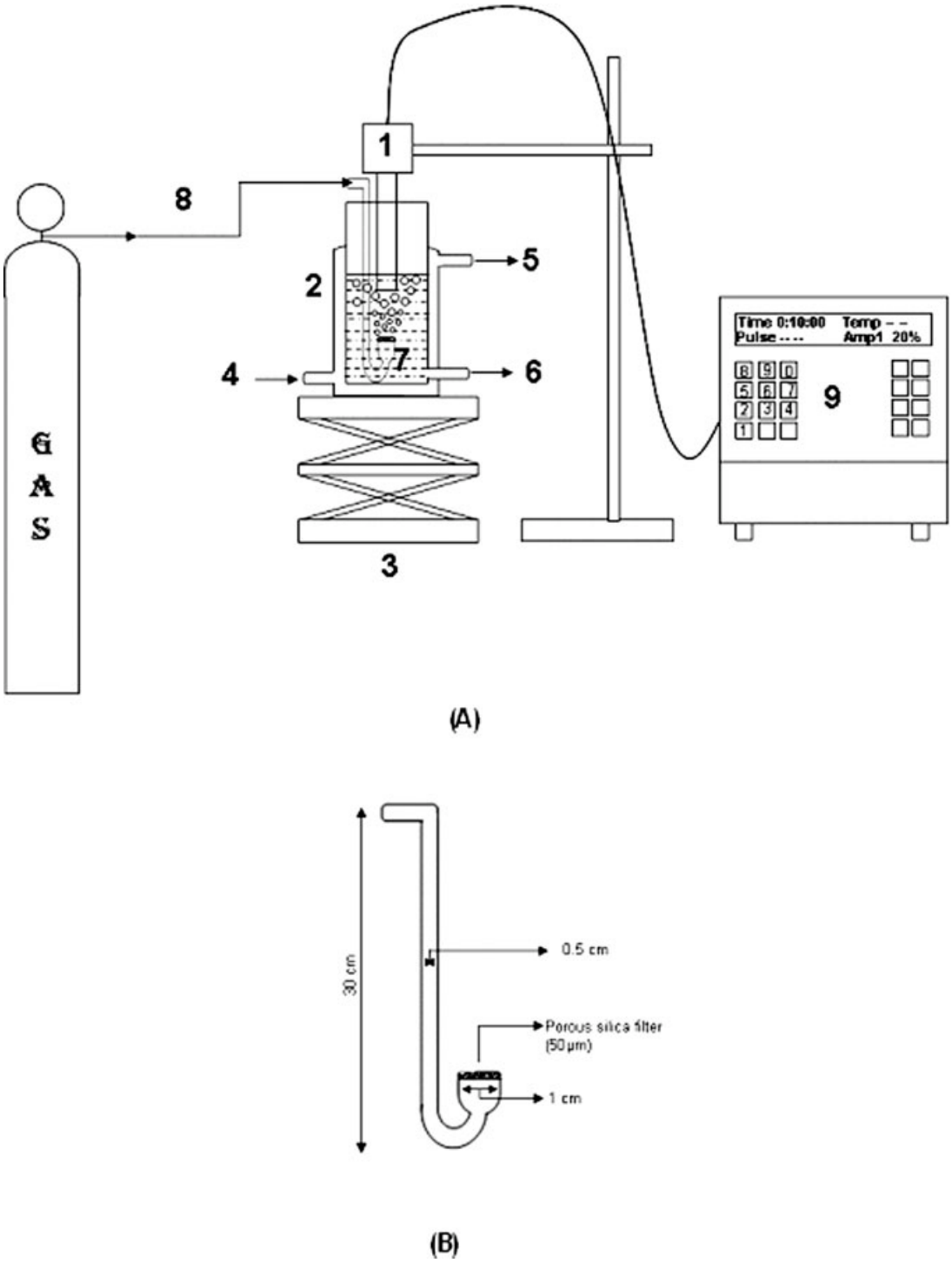

Figure 1. A: Experimental setup: 1, ultrasound horn; 2, jacketed reactor; 3, laboratory jack; 4, cooling water inlet; 5, cooling water outlet; 6, sample withdrawal port; 7, aerator for bubbling of air in the reaction medium; 8, aerator connection to gas storage vessel; 9, control unit of the ultrasound processor; B: the aerator along with dimensions.

try, as explained in greater details in appendix A. In addition, the processor had facility of automatic frequency tuning and amplitude compensation, which ensures constant power delivery to ultrasound probe irrespective of the changes occurring in the liquid medium.

Experimental procedures

Potassium iodide (KI) was bought from Merck (Grade: Pro-analysis) and was used without any pre-treatment. The KI solutions were prepared using water from Millipore (Model: Elix 3). The experiments were carried out in two categories: (1)

degassed medium and (2) saturated medium. In each category the initial concentration of KI was varied as 2, 5, and 10% w/v. Thus, in total there were six sets of experiments. The reproducibility of the results in each set of experiment was assessed with three trials. The reaction temperature was maintained at 28°C during the experiments with reaction volume being 150 ml. The sonication of the reaction medium was done for 10 min with the power output of ultrasonic processor set at 20% of maximum value, as mentioned earlier. During sonication, the temperature of reaction medium was monitored using a digital thermometer. It increased only slightly (~1°C) during the sonication. For the experiments in first category, i.e. degassed reaction medium, the reaction solution was subjected to vacuum for 30 min with intense stirring to reduce the dissolved gas content. For this purpose, a vacuum pump (Riviera, Model: TID-25-S) producing a vacuum of 700 mm Hg (or 60 mm Hg pressure) in the solution was used. By this method, the dissolved oxygen content of the solution could be lowered to 2.7 ppm. This method, however, reduces the free-gas content of the medium as well, leaving the medium not only degassed but also de-nucleated. To compensate for this effect, air was introduced through the aerator during sonication of the degassed KI solutions, so as to provide cavitation nuclei in the medium. The dissolved oxygen content of the reaction medium increased during sonication due to bubbling of air through it. After the completion of the experiment, the dissolved oxygen content of the reaction medium was measured as 4 ppm. However, it is still significantly below the saturation limit (8 ppm). In the second category of experiments, where a saturated medium was used, the dissolved oxygen content of the solution was 7.9 ppm.

Method of analysis

The iodine liberated during sonication was analyzed using a UV–Visible spectrophotometer (Perkin Elmer, Model: Lambda 35). The iodine liberated in the solution forms a complex I_3^- with the iodide ions already present in the KI solution. The UV–Visible spectrum of this complex has a peak at 354 nm. Therefore, the iodine liberation was accounted by monitoring the absorbance values at 354 nm. To quantify the iodine liberation during sonication of KI solutions of various concentrations, calibration of the spectrophotometer was done using KI solutions with known iodine concentrations. For this purpose, the 0.01 N iodine solution was prepared by dissolving the corresponding amount of iodine in a solution with the particular concentration of KI for which calibration had to be done. The concentration of iodine in this solution was determined by titrating against sodium thiosulphate, which was standardized against 0.1 N potassium iodate solution. This standard iodine solution was diluted with the KI solution of same concentration to obtain iodine solutions of different known concentrations. Absorbance values for these solutions were obtained by keeping the un-sonicated or original KI solution of respective concentration as the blank. The calibration curve produced from these values was used estimate the concentration of iodine liberated during various experiments.

Modeling of the Sonochemical Phenomena

It is well known that the species inducing *sonochemistry*, i.e. radicals such as $OH^{\bullet}$, $H^{\bullet}$, $O^{\bullet}$, and $HOO^{\bullet}$ are generated during bubble collapse. However, to date, a direct quantification of this phenomenon is still not possible. One has to rely on the numerical solutions of the bubble dynamics equation to determine the temperature reached during bubble collapse, which is a crucial parameter influencing the extent of radical generation. The other parameter of paramount importance is the amount of water vapor entrapped in the bubble at the time of collapse. This parameter also needs to be determined from bubble dynamics simulations. Modeling of the radicals generation by cavitation bubbles is an active area of research for past three decades and various authors have addressed the matter with different approaches.[19–28]

The most general treatment of the problem of water vapor transport in strongly forced bubble was presented by Storey and Szeri[25] in a landmark paper published in 2000. The principal result of paper by Storey and Szeri was that water vapor transport in the bubble is a two-step process: diffusion to the bubble wall and condensation. Thus, it is influenced by two time scales, viz. the time scale of diffusion (t_{dif}) and the time scale of condensation (t_{cond}), and their magnitudes relative to bubble dynamics (or oscillations) time scale, t_{osc}. In the earlier phases of bubble collapse, $t_{osc} \gg t_{dif}, t_{cond}$, which results in uniform bubble composition. With acceleration of bubble wall, $t_{osc} \ll t_{dif}$, and the water vapor has insufficient time to diffuse to the bubble wall, which results in nearly fixed distribution of water vapor in the bubble. Another mechanism, which traps water vapor in bubble during collapse, is the nonequilibrium phase change at bubble wall, as mentioned earlier. The time scale for the condensation varies inversely with σ_a. Qualitatively, when $t_{osc} \gg t_{cond}$, the condensation is in equilibrium with respect to the bubble motion. On the other hand, when $t_{cond} \gg t_{osc}$, the phase change is nonequilibrium and no water vapor can escape bubble during collapse, causing entrapment of water molecules in the bubble.

The exact mechanism that traps water vapor in the bubble is determined by the relative magnitudes of t_{osc}, t_{dif}, and t_{cond}. When the bubble dynamics time scale is smaller than either the diffusion or condensation time scale, water vapor entrapment occurs. However, both mechanisms can contribute to the water vapor entrapment. Storey and Szeri[26] showed that the condition $t_{osc} \ll t_{dif}$ is reached well before $t_{osc} \ll t_{cond}$. Thus, the phenomenon of water vapor trapping in the cavitation bubble is diffusion limited. In view of the results of Storey and Szeri with full numerical simulations, Toegel et al.[28] developed a diffusion limited model using boundary layer approximation. The existence of boundary layer near bubble wall even at the moment of extremely rapid collapse has been confirmed by other authors as well.[20,29–32] For the validation of this model, Toegel et al.[29] have compared their results with those of Storey and Szeri[25] finding an excellent qualitative and quantitative agreement. For explanation of the sonochemical phenomena we use the model of Toegel et al., which has been described in paragraphs later.

Bubble dynamics

The radial bubble motion is described by the Keller-Miksis equation written as (Brennen[33] and Prosperetti and Lezzi[34]):

$$\left(1-\frac{dR/dt}{c}\right)R\frac{d^2R}{dt^2}+\frac{3}{2}\left(1-\frac{dR/dt}{3c}\right)\left(\frac{dR}{dt}\right)^2 = \frac{1}{\rho_L}\left(1+\frac{dR/dt}{c}\right)(P_i-P_t)+\frac{R}{\rho_L c}\frac{dP_i}{dt}-4\nu\frac{dR/dt}{R}-\frac{2\sigma}{\rho_L R} \quad (1)$$

This is a modification of the Rayleigh-Plesset equation, which takes into account the liquid compressibility. ρ_L, σ, and v denote the physical properties of the liquid medium, viz. the density, surface tension, and kinematic viscosity respectively. c is the speed of sound in the medium. The pressure inside the bubble (P_i) is written using a van der Waals type equation of state as:

$$P_i = \frac{N_{tot}(t)kT}{\left[\frac{4\pi}{3}(R^3(t) - h^3)\right]} \tag{2}$$

Here k is the Boltzmann constant, N_{tot} denotes the total number of molecules in the bubble, which vary according to condensation and evaporation of water vapor, and T is the temperature of bubble contents. h is the van der Waals hard core radius of various species in the bubble, viz. nitrogen, oxygen, and water vapor. Since the hard-core radii of these species differ very little (~5%), we take a common value, $h = R_o/8.86$, for all species, where R_o is the equilibrium radius of the bubble. A simple expression for P_t (the pressure in the bulk liquid driving bubble motion) is written as:

$$P_t = P_o - P_A \sin\ 2\pi ft \tag{3}$$

Here P_o is the ambient pressure and P_A and f denote the pressure amplitude and frequency of the acoustic wave. After substituting $dR/dt = s$, the above equation is transformed into two simultaneous equations:

$$\frac{dR}{dt} = s \tag{4}$$

$$\frac{ds}{dt} = \frac{(1 + s/c)}{R\rho_L(1 - s/c)}(P_i - P_t) + \frac{1}{\rho_L c(1 - s/c)}\frac{dP_i}{dt} - \frac{4vs}{R^2(1 - s/c)} - \frac{2\sigma}{\rho_L R^2(1 - s/c)} - \frac{3}{2}\frac{s^2(1 - s/3c)}{R(1 - s/c)} \tag{5}$$

Mass transfer across bubble

During bubble oscillations, both gas and water vapor diffuse across the bubble wall. The time scale for the diffusion of gas can be given as $\sim R_o^2/D$, where D is the diffusion coefficient. For representative values as $R_o \sim 10$ μm and $D \sim 10^{-9}$ m^2/s, the time scale for the gas diffusion is 0.1 ms, which is far higher than time scale of bubble dynamics (which is same as time scale of ultrasound wave: 50 μs for 20 kHz wave). Thus, the transport of gas across bubble in one acoustic cycle can be ignored. However, gas transport across the bubble over larger time duration needs to be accounted for. Depending on the amplitude of the ultrasound wave driving the bubble motion and the extent of saturation of the liquid medium, the bubble may grow or shrink during oscillations because of transport of gas across the bubble. This process is called rectified diffusion, which has been investigated over past several decades for small amplitude oscillations of the bubble.[35–37] More recently, a generalized formulation of rectified diffusion is given by Lofstedt et al.[38] and Fyrillas and Szeri,[39] which can be applied to large amplitude nonlinear motion of bubbles driven by the ultrasound waves of pressure amplitude greater than transient cavitation threshold (typically > 1 bar for bubbles of size 5–20 μm). The major conclusions of the study of Lofstedt et al.[38] and Fyrillas and Szeri[39] in the context of the present study is as follows: For acoustic pressure amplitudes > 1 atm, the bubble grows during oscillations if the liquid medium is relatively saturated (≥80% or so). On the other hand, if the medium is unsaturated (relative saturation ≤ 30% or so) the bubble shrinks during radial motion. While choosing parameters for simulation of the radial bubble motion, we make use of these conclusions. For greater details on the mathematical analysis of rectified diffusion, we refer the reader to the original papers of Lofstedt et al.[38] and Fyrillas and Szeri.[39]

Diffusion of the water vapor across the bubble wall shows interesting features, as already discussed earlier. During bubble oscillations the surface temperature of the bubble exceeds bulk water temperature only for a very brief moment during collapse. On this basis, the bubble can be divided into two parts: (i) a "cold" boundary layer in thermal equilibrium with liquid, and (ii) a hot homogeneous core. Of course, this distinction assumes that the condensation of water molecules at the bubble wall is fast enough to maintain equilibrium. The instantaneous diffusive penetration depth using dimensional analysis is taken to be: $l_{diff} = \sqrt{Dt_{osc}}$, where t_{osc} is the time scale of bubble oscillations: $R/|dR/dt|$.

On the basis of the fact that the water vapor transport is always diffusion limited, the rate of change of water molecules in the bubble (N_W) is given by:

$$\frac{dN_W}{dt} = 4\pi R^2 D \frac{\partial C_W}{\partial r}\Big|_{r=R} \approx 4\pi R^2 D\left(\frac{C_{WR} - C_W}{l_{diff}}\right) \tag{6}$$

where C_{WR} is the equilibrium concentration of water molecules at the bubble wall, calculated using vapor pressure at the bulk temperature (T_o) and C_W is the actual concentration of the water molecules in the bubble core.

Upper limit on diffusion length: The above analysis holds good for bubble in motion, where the bubble wall velocity, dR/dt, has a nonzero value. However, at the instances of maximum and minimum radius, the bubble wall velocity is zero and we need an alternate expression for the diffusion length. For this purpose, we identify that for $dR/dt = 0$ the equation for water vapor transport inside the bubble becomes a pure diffusion equation:

$$\frac{\partial C_W}{\partial t} = D\left(\frac{\partial^2 C_W}{\partial r^2} + \frac{2}{r}\frac{\partial C_W}{\partial r}\right) \tag{7}$$

with boundary conditions: (1) $r = 0$, $\partial C_W/\partial t = 0$ for $t \geq 0$; (ii) $r = R$, $C_W = C_{WR}$ for $t \geq 0$; (iii) $C_W = C_{W0} = 0$ for $t = 0$ and $0 \leq r \leq R$. The analytical solution to the above problem is given by Crank[40]:

$$\frac{C_W - C_{W0}}{C_{WR} - C_{W0}} = 1 + \frac{2R}{\pi r}\sum_{n=1}^{\infty}\frac{(-1)^n}{n}\sin\left(\frac{nr}{R/\pi}\right)\exp\left(-\frac{n^2 Dt}{(R/\pi)^2}\right) \tag{8}$$

Table 1. Thermodynamic Properties of Various Species

Species	Degree of Freedom (f_i)	Molecular Specific Heat (C_p)	Molecular Specific Heat (C_v)
N_2	5	$\frac{7}{2}$k	$k\left(\frac{5}{2}+\frac{\left(\theta_{N_2}/T\right)^2\exp\left(\theta_{N_2}/T\right)}{\left(\exp\left(\theta_{N_2}/T\right)-1\right)^2}\right)$
O_2	5	$\frac{7}{2}$k	$k\left(\frac{5}{2}+\frac{\left(\theta_{O_2}/T\right)^2\exp\left(\theta_{O_2}/T\right)}{\left(\exp\left(\theta_{O_2}/T\right)-1\right)^2}\right)$
H_2O	6	4k	$k\left(3+\sum_i^3\frac{\left(\theta_{i,H_2O}/T\right)^2\exp\left(\theta_{i,H_2O}/T\right)}{\left(\exp\left(\theta_{i,H_2O}/T\right)-1\right)^2}\right)$

The vibrational temperatures of various species are as follows: $\theta_{N_2} = 3350$ K, $\theta_{O_2} = 2273$ K, $\theta_{1,H_2O} = 2295$ K, $\theta_{2,H_2O} = 5255$ K, $\theta_{3,H_2O} = 5400$ K.

From the inspection of the above solution, the characteristic length for the diffusion is R/π. We choose this as the upper limit for the diffusion length. Thus:

$$l_{\text{diff}} = \min\left(\sqrt{\frac{RD}{|dR/dt|}}, \frac{R}{\pi}\right) \tag{9}$$

Estimation of the diffusion coefficient for water vapor in the ternary system nitrogen–oxygen–water on the basis of Chapman-Enskog theory[41] is explained later.

Heat transfer across bubble

With complete analogy with mass transfer, the heat transfer across the bubble wall is:

$$\frac{dQ}{dt} = 4\pi R^2 \lambda \left(\frac{T_o - T}{l_{\text{th}}}\right) \tag{10}$$

where, λ is the thermal conductivity of the bubble contents and l_{th} is the thermal diffusion length: $\min\left(\frac{R}{\pi}, \sqrt{\frac{R\kappa}{|dR/dt|}}\right)$. Thermal diffusivity κ is calculated as: $\kappa = \frac{\lambda}{\rho_{\text{mix}} C_{\text{p,mix}}}$, where, $\rho_{\text{mix}} C_{\text{p,mix}} = \sum_{i=1}^{n} \rho_i C_{\text{pi}}$. The densities ρ_i of the various species present in the bubble are expressed in terms of molecules/m^3 and C_{pi} are the molecular specific heats. The C_p values for various species, viz. nitrogen, oxygen, and water, are listed in Table 1. Calculation of the effective thermal conductivity of the mixture of these three species is explained later.

Overall energy balance

Treating bubble as an open system, the overall energy balance for the bubble contents is written as:

$$\frac{dE}{dt} = \frac{dQ}{dt} - \frac{dW}{dt} + h_W \frac{dN_W}{dt} \tag{11}$$

However, the total energy E is a function of the temperature and volume of the bubble, and the number of molecules of various species in it. Thus, the rate of change of E for the air bubbles is written as:

$$\frac{dE}{dt} = \left(\frac{\partial E}{\partial N_W}\right)_{N_{N_2},N_{O_2},V,T}\frac{dN_W}{dt} + \left(\frac{\partial E}{\partial N_{N_2}}\right)_{N_W,N_{O_2},V,T}\frac{dN_{N_2}}{dt} + \left(\frac{\partial E}{\partial N_{O_2}}\right)_{N_W,N_{N_2},V,T}\frac{dN_{O_2}}{dt} + \left(\frac{\partial E}{\partial T}\right)_{N_W,N_{N_2},N_{O_2},V}\frac{dT}{dt} + \left(\frac{\partial E}{\partial V}\right)_{N_W,N_{N_2},N_{O_2},T}\frac{dV}{dt} \tag{12}$$

where, V is the volume of the bubble and N_{N_2}, N_{O_2}, and N_W are the number of nitrogen, oxygen, and water molecules in the bubble, respectively. Per the discussion for rectified diffusion given earlier, for a few acoustic cycles, we neglect the transport of gases during the radial motion of bubble. Thus, $dN_{N_2}/dt = dN_{O_2}/dt = 0$. The enthalpy of the water molecule entering the bubble from "cold" interface is: $h_W = 4$ kT$_o$. The specific energy of the water molecule in the bubble is the thermal energy U_W and is written as:

$$\left(\frac{\partial E}{\partial N_W}\right) = U_W = N_W kT\left(3 + \sum \frac{\theta_i T}{\exp(\theta_i/T) - 1}\right) \tag{13}$$

Here θ_i are the characteristic vibrational temperatures, values of which for various species are listed in Table 1. The rate of work done by the bubble (dW/dt) reduces to expansion work: P_i dV. Comparing equations 11 and 12, and identifying that $(\partial E/\partial T) = C_v$ and $(\partial E/\partial V) = 0$, as internal energy of an ideal gas is mainly a function of its composition and temperature, we can now write another equation for the change of the temperature of the bubble:

$$C_{v,\text{mix}}\frac{dT}{dt} = \frac{dQ}{dt} - P_i dV + (h_W - U_W)\frac{dN_W}{dt} \tag{14}$$

The specific heat of the mixture $C_{v,\text{mix}}$ is written in terms of the molecular specific heats of individual components ($C_{v,i}$) and the number of molecules of individual components (N_i) as:

$$C_{v,\text{mix}} = \sum_{i=1}^{N} C_{v,i} N_i \tag{15}$$

The C_v values for various species, viz. nitrogen, oxygen, and water are listed in Table 1.

Transport parameters for air–water vapor mixture

In case of air–water vapor mixture, we encounter a ternary system: nitrogen–oxygen–water vapor. To determine the diffusion coefficient for water vapor in this system, we first calculate the binary diffusion coefficients for N_2-H_2O and O_2-H_2O mixtures. Diffusion coefficient of species 1 in the mixture of two species 1–2, to a first approximation is written as[42]:

$$D = \frac{3}{8}\frac{\sqrt{\pi kT/\mu_{12}}}{n_{12}\pi\sigma_{12}^2\Omega_{12}^{(1,1)*}} \tag{16}$$

m_1 and m_2 are the molecular masses of species 1 and 2 respectively, and $\mu_{12} = 2\ m_1 m_2/(m_1 + m_2)$ is the reduced

molecular mass of the two species. $n_{12} = n_1 + n_2$ is the joint concentration of the two species. σ_{12} is a parameter in the potential function characteristic of 1–2 interaction. It is approximated as $(\sigma_1 + \sigma_2)/2$, where σ_1 and σ_2 are the molecular diameters of water and argon. $\Omega_{12}^{(1,1)*}$ is a dimensionless correction of first order that describes the deviation of the collisional cross-section from the hard sphere cross-section. Values of this parameter are given by Hirschfelder et al.[41] as a function of the reduced temperature of the two species: $T_{12}^{*} = \sqrt{[T/(\varepsilon/k)]_1[T/(\varepsilon/k)]_2}$. Values of the potential parameter (ε/k) for various species (in K) are available in various texts.[41,43] The overall diffusion coefficient for water vapor in ternary mixture is calculated as[41]:

$$\frac{1}{D} = \frac{\varepsilon_{N_2}}{(1-\varepsilon_{H_2O}) + D_{N_2-H_2O}} + \frac{\varepsilon_{O_2}}{(1-\varepsilon_{H_2O})D_{O_2-H_2O}} \tag{17}$$

where ε represents mole fraction of the respective species at the bubble wall. For the determination of conductivity of the ternary mixture, the viscosity of various individual species is evaluated as[41]:

$$\eta = \frac{5}{16}\frac{\sqrt{\pi m k T}}{\pi\sigma^2\Omega^{(2,2)*}} \tag{18}$$

Thereafter, the conductivity of the species is related to its viscosity using the Eucken correction formula:

$$\lambda = \frac{15k}{m}\eta\left(\frac{4f_i}{30} + \frac{3}{5}\right) \tag{19}$$

where f_i is the number of degree of freedom for the species at the bubble wall. Values of f_i for various species are listed in Table 1. The effective heat conductivity of the ternary mixture is then constructed from individual conductivities as[42]:

$$\lambda_{mix} = \sum_i \frac{\varepsilon_i\lambda_i}{\sum_j \varepsilon_j\phi_{i,j}} \tag{20}$$

$$\phi_{i,j} = \frac{1}{\sqrt{8}}\left(1 + \frac{m_i}{m_j}\right)^{-1/2}\left(1 + \left(\frac{n_i}{n_j}\right)^{-1/2}\left(\frac{m_i}{m_j}\right)^{1/4}\right)^2 \tag{21}$$

where $i, j = N_2$, O_2, and H_2O.

Estimating the physical parameters for aqueous KI solutions

The liquid medium in the present case is aqueous solution of potassium iodide. The physical properties of water (such as vapor pressure and surface tension) change with addition of KI. To obtain the vapor pressure of water in KI solution, we are following expression given by Horvath[44]:

$$\phi = \frac{x-1}{x}\left[\ln(1-x) - 1.1517x + 0.0148\sqrt{x} + 3.204x^{3/2} - 11.44x^2\right] \tag{22}$$

where ϕ is the osmotic coefficient and x, the mole fraction of KI in the solution. In terms of concentration of KI (C_{KI}, in mol/lit), x is written as:

$$x = \frac{C_{KI}}{C_{KI} + 55.51} \tag{23}$$

The relation between ϕ, the vapor pressure pure water P_{H_2O} and the vapor pressure of water in KI solution P_v is given as:

$$\phi = \left[\frac{-1000}{36C_{KI}}\right]\ln(P_v/P_{H_2O}) \tag{24}$$

The vapor pressure of pure water (in mm Hg) at temperature T (in K) is calculated using Antoine's equation:

$$\ln P_{H_2O} = 18.3036 - \frac{3816.44}{T - 46.13} \tag{25}$$

A quick inspection of Eqs. 22–25 reveals that the vapor pressure of water is lowered with addition of KI. We refer to this result later in the paper. The surface tension of water increases with dissolution of KI. The surface tension of the aqueous KI solution has been correlated to the KI concentration (C_{KI}, in mol/lit) as[17]:

$$\sigma = \sigma_{H_2O} + \frac{142.3616}{100,000}C_{KI} \tag{26}$$

σ_{H_2O} is the surface tension of pure water taken to be 0.07272 N/m.

Numerical solution

The Eqs. 4, 5, 6, and 14 constitute the complete formulation for the radial motion of bubble, which can be solved simultaneously using Runge-Kutta adaptive step size method.[45] We would like to mention that the phenomenon of bubble collapse (or bubble fragmentation) depends on many factors such as the surface instability, local flow conditions, and the bubble population in the vicinity of the bubble. For the conditions of maximum surface instability and flow instability, the bubble collapses (or fragments) at the first compression after an initial expansion. Considering this, the condition for bubble collapse is taken as the first compression after an initial expansion. Four important parameters required for the simulation of bubble dynamics equation are frequency (f) and pressure amplitude (P_A) of ultrasound, vapor pressure of water (P_{H_2O}), and the equilibrium bubble radius (R_o).

Frequency. The frequency of the ultrasound was taken as 20 kHz, same as the frequency of the ultrasound processor used in the experiments.

Pressure Amplitude. Using calorimetric method based on the actual power consumption of the processor and the cross-sectional area of the ultrasound probe tip, the amplitude of ultrasound wave emitted by the probe was calculated as 1.5 bar (for greater details on calculation of acoustic pressure amplitude, refer to appendix). The ultrasound wave undergoes attenuation as it propagates through the medium, and hence, the acoustic pressure amplitude actually experienced by the bubble is smaller than 1.5 bar. This attenuation varies directly with the size and population density of bubbles

(number of bubbles per unit volume of liquid).[46] In a nondegassed medium, the attenuation of ultrasound wave is higher due to larger size and larger population of bubbles. Therefore, for the simulation of radial bubble motion in a nondegassed medium, we use a value $P_A = 1.25$ bar, which accounts for the attenuation effect. For a degassed medium, the attenuation effect is negligible and a value $P_A = 1.5$ bar is used for simulations.

Equilibrium Bubble Radius. The equilibrium radius of the bubbles is difficult to estimate. Moreover, it keeps on changing due to phenomenon of rectified diffusion during oscillations. Typically for $P_A > 1$ bar, the bubble shrinks during oscillations in a highly unsaturated medium, while in a relatively saturated medium it grows due to process of rectified diffusion. In the first category of experiments, the dissolved gas content of the medium (represented by the dissolved oxygen content) changed during sonication from 2.7 to 4 ppm of dissolved oxygen. Even with this rise in dissolved gas content, the medium is still well below saturation (8 ppm of dissolved oxygen), which makes a bubble shrink during its oscillations due to rectified diffusion. Thus, the overall physics of cavitation bubble in the degassed reaction medium remains unaffected during the sonication period. Therefore, we have chosen two equilibrium sizes of bubbles for simulation: a smaller size of 10 μm representing bubbles in the degassed medium, while a larger size of 20 μm representing bubbles in the nondegassed medium.

Vapor Pressure of Water. The vapor pressure of pure water has been calculated using the initial temperature of the solution (28°C), while the reduction in vapor pressure due to KI has been calculated using Eqs. 22–24. As mentioned in appendix, the temperature of the solution rises by about 1°C during sonication. As the vapor pressures of water at 28 and 29°C differ by <5%, we have ignored the temperature rise during simulations. One can also use an average of initial and final temperatures for calculations; however, this makes trivial quantitative changes to the simulation results and the trends of the results remain unchanged. It needs to be mentioned that although vapor pressure of pure water rises slightly during reaction, the reduction due to KI remains the same, as this factor is only a function of KI concentration in the medium. Since the KI concentration in the medium remains practically the same during 10 min of sonication, the reduction in vapor pressure also stays the same.

While calculating the composition of the bubble at the time collapse, we assume that thermodynamic equilibrium is attained. This assumption is based on the relative magnitudes of bubble collapse time scale and time scale of various radical reactions. The time scale of bubble collapse is of the order of a few tens of nanoseconds ($\sim 10^{-8}$ s, Storey and Szeri[25]], while time scale of radical reactions is at least two orders of magnitude smaller ($\sim 10^{-10}$ s, Krishnan et al.[47]]. Thus, thermodynamic equilibrium should prevail till the point of minimum radius during collapse. The equilibrium mole fraction of the various species in the bubble (i.e. H_2O, H_2, O_2, $H^{\bullet}$, $OH^{\bullet}$, $O^{\bullet}$, H_2O_2, $HOO^{\bullet}$, O_3) at the conditions of temperature and pressure at first the compression of the bubble was calculated using software FACTSAGE, which uses the free-energy minimization algorithm proposed by Eriksson.[48]

Results and Discussion

The iodine liberation during sonication depends on the amount of radical species produced by the cavitation bubbles, which in turn depends on two factors: (1) the extent of water vapor entrapped in the bubble at the time of collapse, and (2) the temperature peak attained during collapse, which decides the equilibrium composition of various species resulting out of dissociation of water vapor entrapped in the bubble. These two factors can be evaluated from solution of bubble dynamics equation. The yield of KI oxidation reaction can be defined as: number of moles of iodine liberated per unit time-per unit reaction volume-per unit mole of KI-per unit power input to system. However, the power input, sonication time and reaction volume were same for all experiments, and thus, the definition of sonochemical yield reduces to moles of iodine liberated per unit mole of KI. As stated earlier, an important parameter that influences the yield of sonochemical reaction is the probability of interaction between radical and reactant molecule. The higher the concentration of reactant molecules the greater the probability of interaction. Therefore, in case of relatively dilute solutions, the radicals produced by cavitation bubbles undergo recombination without inducing any chemical reaction, as the probability of radical–reactant interaction is low. With this preamble, we present the experimental and simulation results.

Trends in sonochemical yield with different experimental parameters are shown in Figure 2. Out of all combinations of reaction conditions attempted, the highest yield is obtained for 2% w/v KI solution with degassed reaction medium, while the lowest yield is seen for 10% w/v KI concentration with nondegassed reaction medium. For either degassed or nondegassed medium, the yield decreased with increasing KI concentration. For all initial concentrations of KI (2, 5, and 10% w/v), yield increased by about 50% with degassing of the reaction medium. However, an interesting observation is that the absolute amount of iodine liberated during sonication increases with increasing KI concentration in the medium.

Illustrative simulations of radial motion of air bubbles with $R_o = 10$ and 20 μm in 10% w/v KI solution are shown in Figures 3 and 4 respectively. The summary of entire simulation results for KI solutions of 2, 5, and 10% w/v concentration is given in Table 2. This table lists the collapse

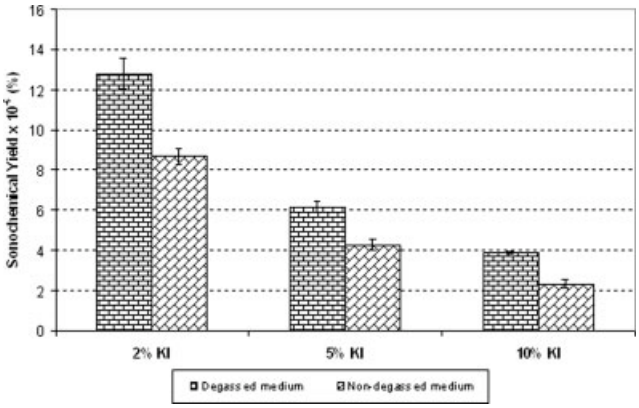

Figure 2. Experimental results on iodine liberation under various reaction conditions.

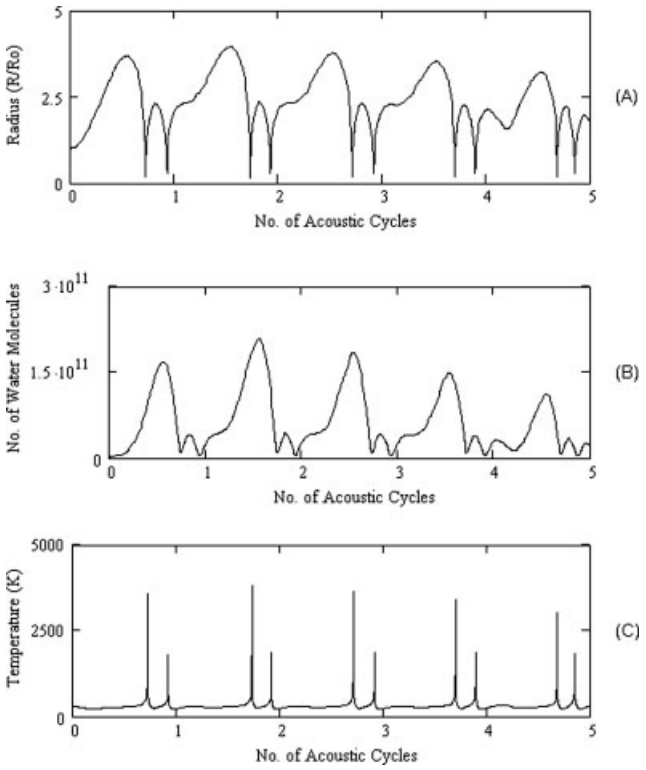

Figure 3. Simulation of the radial motion of 10 μm air bubble (representative of degassed medium) in 10% w/v KI solution.

Time variation of (A) normalized bubble radius (R/R_o); (B) number of water molecules in the bubble; (C) temperature in the bubble.

conditions (i.e. number of water molecules entrapped in the bubble and temperature peak reached in the bubble during collapse) and the equilibrium composition of the bubble contents. It is evident that OH is the dominant radical species produced in the bubble. The total number of OH radicals produced per single bubble can be calculated by the product of the number of water molecules entrapped and the equilibrium mole fraction. The OH radical contributes to the oxidation of KI to liberate iodine through reaction[49]: $2\ KI + 2OH^{\cdot} \rightarrow 2\ KOH + I_2$. From the simulation results presented in Table 2, certain trends in OH radical yield per single bubble with varying gas content and initial KI concentration in the medium can be observed and explained as follows:

- The highest yield of OH radicals per single bubble is seen for 2% w/v KI solution and initial bubble size of 10 μm—representative of degassed medium. With increasing KI concentration (5 and 10% w/v), the temperature peak reached during collapse of a 10 μm bubble shows small variation; however, the extent of water vapor entrapment reduces. Consequence of this is the reduction in the yield of OH radicals per bubble. Similar trend is seen for 20 μm bubble (representing nondegassed medium) for all KI concentrations. This trend can be explained as follows: with increasing concentration of KI, the vapor pressure of water reduces. This reduces the diffusive flux of water molecules across a bubble, which is directly proportional to vapor pressure of water at bubble interface, as described by Eq. 6. Reduction in the flux of water molecules also reduces the extent of water vapor entrapment in the bubble during collapse.
- For a given initial KI concentration (either 2, 5, or 10% w/v) the OH radical production increases with degassing of the medium. This is a combined effect of rectified diffusion and pressure amplitude of the ultrasound wave. As mentioned earlier, in a degassed medium, the process of rectified diffusion makes a bubble shrink as it oscillates under influence of ultrasound wave. A smaller bubble undergoes greater compression during collapse, giving higher peak temperatures. In addition, the attenuation of ultrasound wave is much smaller in a degassed medium, and hence, the pressure amplitude of ultrasound wave actually experienced by a bubble is high that makes the bubble collapse even more intense. This results in larger equilibrium composition of OH radicals resulting out of dissociation of entrapped water molecules in the bubble during collapse. On the contrary, in a nondegassed medium, ultrasound wave undergoes attenuation, as mentioned earlier. Moreover, rectified diffusion makes the bubble grow during oscillations. These two effects reduce the intensity of bubble collapse yielding lower peak temperatures, and hence, lesser production of OH radicals from the entrapped water molecules.

Comparison of the experimental and simulations result reveals that the trend in sonochemical yield with varying gas content of the medium and initial KI concentration exactly

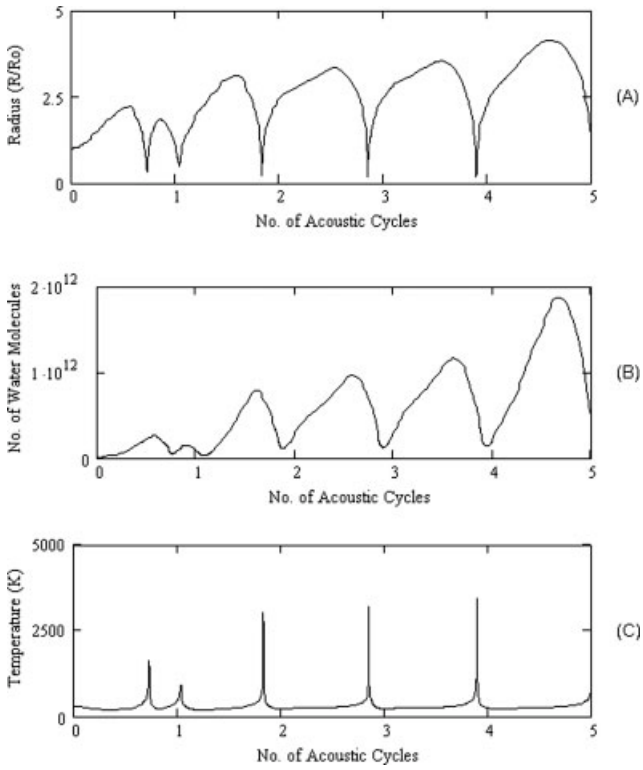

Figure 4. Simulation of the radial motion of 20 μm air bubble (representative of nondegassed medium) in 10% w/v KI solution.

Time variation of (A) normalized bubble radius (R/R_o); (B) number of water molecules in the bubble; (C) temperature in the bubble.

Table 2. Simulation Results For Air Bubble

	Parameters for simulations					
	$R_o = 10\ \mu m$ 2% w/v KI soln.	$R_o = 20\ \mu m$ 2% w/v KI soln.	$R_o = 10\ \mu m$ 5% w/v KI soln.	$R_o = 20\ \mu m$ 5% w/v KI soln.	$R_o = 10\ \mu m$ 10% w/v KI soln.	$R_o = 10\ \mu m$ 10% w/v KI soln.
	Conditions at the first compression of the bubble					
	$T_{max} = 3607$ K $N_{WT} = 2.23E{+}010$	$T_{max} = 1745$ K $N_{WT} = 1.82E{+}011$	$T_{max} = 3620$ K $N_{WT} = 2.08E{+}010$	$T_{max} = 1832$ K $N_{WT} = 1.10E{+}11$	$T_{max} = 3587$ K $N_{WT} = 1.89E{+}010$	$T_{max} = 1639$ K $N_{WT} = 9.35E{+}010$
	Equilibrium composition of different radical species in the bubble at collapse (mol fraction)					
O_2	4.9626E−01	6.2215E−01	5.1293E−01	6.2506E−01	5.3766E−01	6.6243E−01
H_2O	4.3902E−01	3.7750E−01	4.2179E−01	3.7437E−01	4.0059E−02	3.3740E−01
OH•	4.9454E−02	3.0761E−04	4.9678E−02	4.9968E−04	4.6981E−02	1.5198E−04
O•	6.2549E−03	3.2991E−06	6.5203E−03	6.9819E−06	6.294E−03	1.2329E−06
HOO•	5.8932E−03	3.3273E−05	6.0149E−03	5.2046E−05	5.7159E−03	1.7856E−05
H_2	1.8079E−03	8.3585E−07	1.7609E−03	1.7212E−06	1.5607E−03	2.6895E−07
H_2O_2	8.3459E−04	3.6320E−06	8.2776E−04	5.6382E−06	7.5433E−04	1.8173E−06
H•	4.2632E−04	1.1996E−08	4.2973E−04	3.3064E−08	3.8492E−04	2.8041E−09
O_3	5.0750E−05	1.1775E−07	5.434E−05	2.0710E−07	5.492E−05	6.0263E−08
					Net amount of hydroxyl radicals produced per bubble	
N_{OH}	1.1028E+09	5.5985E+07	1.0333E+09	5.4965E+07	8.8794E+08	1.4210E+07

The number format is as follows: 4.9454E−02 should be read as 4.9454×10^{-2}. Species having equilibrium mole fraction less than 10^{-20} have been ignored. Species with Nitrogen as a constituent element have been ignored, as they are found in traces and have no contribution in the context of radical chemistry for oxidation of KI. An equilibrium bubble size (R_o) of 10 μm represents degassed KI solution while an equilibrium bubble size of 20 μm represents nondegassed solution. Various notations used are as follows: T_{max}, temperature peak reached in the bubble at the time of first collapase; N_{WT}, number of water molecules trapped in the bubble at the instance of first collapse.

follows the trends in OH radical production per single bubble. It is thus evident that the physical technique of degassing the medium is far more efficient in enhancing the sonochemical yield than the chemical technique of increasing initial KI concentration. As already pointed out, the absolute amount of iodine liberated during sonication increases with increasing initial KI concentration. Explanation for this effect can be given on the basis of probability of interaction between radicals generated by cavitation bubbles and the KI molecules. This probability varies directly with the concentration of KI in the order 2 wt % < 5 wt % < 10 wt %. Therefore, in 10 wt % KI solution, the utilization of OH radicals for induction of chemical reaction is higher, although the net generation of OH radical is lesser. On the other hand, for 2 wt % KI solution the probability of radical–reactant interaction is low, and thus, sizeable fraction of radicals may undergo mere recombination without any reaction albeit net generation of radicals is higher. One can easily perceive that if the probability of radical–reactant interaction was same for all concentrations of KI, absolute iodine liberation would have been the highest for 2 wt % KI solution.

In addition to the comparative evaluation of physical and chemical techniques for enhancement of sonochemical yield; this study also brings to light some interesting mechanistic features of a sonochemical reaction. The influence of various parameters on a sonochemical reaction is revealed to be highly interdependent. The yield of such a reaction strongly depends on the physical acoustics of the system. The major influencing parameter in this regard turns out to be the dissolved gas content of the medium, which manifests its effect through the process of rectified diffusion and attenuation that affects two other important parameters, viz. the equilibrium bubble radius and the amplitude of the ultrasound wave, which ultimately affect the intensity of cavitation bubble collapse and the production of OH radicals from the bubble. On the other hand, initial reactant concentration turns out to be a counter-productive parameter. Because of reduction in the vapor pressure of water with increasing KI concentration, the important phenomenon of water vapor trapping in the cavitation bubble during collapse—subsequently leading to radical production through dissociation—is adversely affected. The exact mechanism of the influence of dissolved gas content and initial KI concentration on the sonochemical yield, which can be worked out from the results and analysis presented above is shown in Figure 5.

Conclusion

In this article, we have tried to illuminate the complex interrelations between the physics and chemistry of a sonochemical reaction system, i.e. the physical phenomena of bubble dynamics and its chemical manifestation, which is formation of radicals that induce chemical reaction in the medium. With experiments using a well-known sonochemical reaction and a mathematical model that takes into account the essential physics of the bubble dynamics, we have shown as how the macroscopic manifestation (i.e. the sonochemical yield) of the microscopic phenomena (i.e. transient collapse of cavitation bubble) is a complicated function of several inter-dependent physical processes such as rectified diffusion, water vapor transport and entrapment in cavitation bubbles and the ultrasound wave attenuation. Degassing of the reaction medium intensifies the transient collapse of the cavitation bubble, resulting in higher production of OH and other radicals, which enhance the yield of the sonochemical reaction. Quite unexpectedly, increasing the initial reactant concentration has an adverse effect on the sonochemical yield. This is a consequence of the lessening of the radical produc-

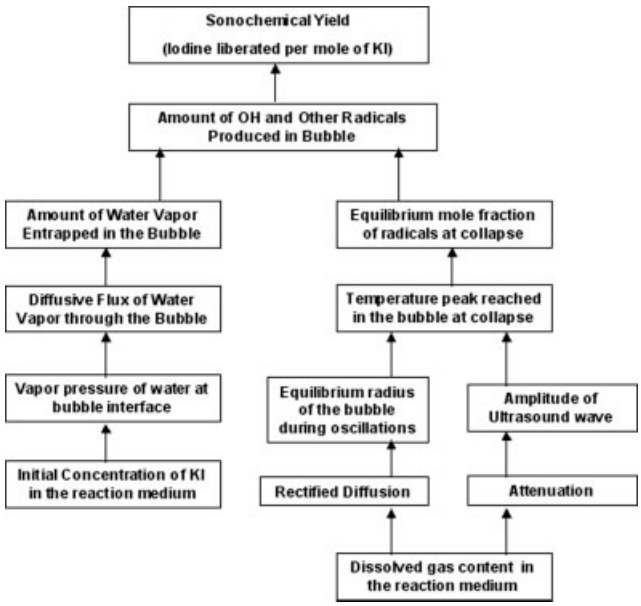

Figure 5. The exact mechanism of influence of dissolved gas content and initial KI concentration on sonochemical yield, which can be worked out from the results and analysis presented in this study.

tion by cavitation bubbles due to decrease in the vapor pressure of water at the bubble interface with increasing initial reactant concentration. An important conclusion of this study is that extent of water vapor entrapment in the bubble and the intensity of the transient cavitation bubble collapse are the principal physical phenomena that affect the yield of a sonochemical reaction. All reaction parameters, such as initial reactant concentration and dissolved gas content of the reaction medium manifest their influence on the sonochemical yield through these physical phenomena. Therefore, any attempt to maximize the sonochemical yield by variation of any reaction parameter should take into account the influence of that parameter on the above-mentioned physical phenomena. The present study puts forth a framework for such an attempt with the model reaction of oxidation of potassium iodide, which can be extended to any other sonochemical reaction system.

Acknowledgments

Authors gratefully acknowledge valuable suggestions from Dr. Brian Storey (Department of Mechanical Engineering, Franklin W. Olin College of Engineering, USA) and Professor Andrea Prosperetti (Department of Mechanical Engineering, John Hopkins University, USA). This work was supported by Department of Science and Technology (DST), Government of India under Fast Track Scheme for Young Scientists.

Literature Cited

1. Suslick KS. *Ultrasound: Its Physical, Chemical and Biological Effects*. New York: VCH, 1988.
2. Mason TJ, Lorimer JP. *Sonochemistry: Theory, Application and Uses of Ultrasound in Chemistry*. New York: Ellis Horwood, 1989.
3. Shah YT, Pandit AB, Moholkar VS. *Cavitation Reaction Engineering*. New York: Plenum Press, 1999.
4. Moholkar VS, Warmoeskerken MMCG. An integrated approach to optimization of an ultrasonic processor. *AIChE J* 2003;49:2918–2932.
5. Moholkar VS, Warmoeskerken MMCG, Ohl CD, Prosperetti A. The mechanism of mass transfer enhancement in textile with ultrasound. *AIChE J* 2004;50:58–64.
6. Tuziuti T, Yasui K, Iida Y, Taoda H, Koda S. Effect of particle addition on sonochemical reaction. *Ultrasonics* 2004;42:597–601.
7. Tuziuti T, Yasui K, Sivakumar M, Iida Y, Miyoshi N. Correlation between acoustic cavitation noise and yield enhancement of sonochemical reaction by particle addition. *J Phys Chem A* 2005; 109:4869–4872.
8. Kirpalani DM, McQuinn KJ. Experimental quantification of cavitation yield revisited: focus on high frequency ultrasound reactors. *Ultrason Sonochem* 2006;13:1–5.
9. Seymour JD, Wallace HC, Gupta RB. Sonochemical reaction at 640 kHz using an efficient reactor. Oxidation of potassium iodide. *Ultrason Sonochem* 1994;1:S75–S79.
10. Entezari MH, Kruus P. Effect of frequency on sonochemical reactions. I. Absolute rates. *Ultrason Sonochem* 1994;1:75–79.
11. Entezari MH, Kruus P. Effect of frequency on sonochemical reactions. II. Temperature and intensity effects. *Ultrason Sonochem* 1996; 3:19–24.
12. Shirgaonkar IZ, Pandit AB. Degradation of aqueous solution of potassium iodide and sodium cyanide in the presence of carbon tetrachloride. *Ultrason Sonochem* 1997;4:245–253.
13. Gutierrez M, Henglein A, Ibanez F. Radical scavenging in the sonolysis of aqueous solutions of iodide, bromide and azide. *J Phys Chem* 1991;95:6044–6047.
14. Henglein A, Gutierrez M. Chemical effects of continuous and pulsed ultrasound: a comparative study of polymer degradation and iodide oxidation. *J Phys Chem* 1990;94:5169–5172.
15. Gogate PR, Shirgaonkar IZ, Sivakumar M, Senthil kumar P, Vichare NP, Pandit AB. Cavitation reactors: efficiency assessment using a model reaction. *AIChE J* 2001;47:2526–2538.
16. Gogate PR, Mujumdar S, Pandit AB. Large scale sonochemical reactors for process intensification: design and experimental validation. *J Chem Technol Biotechnol* 2003;78:685–693.
17. Prasad Naidu DV, Rajan R, Kumar R, Gandhi KS, Arakeri VH, Chandrasekaran S. Modeling of a batch sonochemical reactor. *Chem Eng Sci* 1994;49:877–888.
18. Flynn HG. Physics of acoustic cavitation in liquids. In: Mason WP, editor. *Physical Acoustics*. New York: Academic Press, 1964:57–172.
19. Kamath V, Prosperetti A, Egolfopoulos FN. A theoretical study of Sonoluminescence. *J Acoust Soc Am* 1993;94:248–260.
20. Gong C, Hart DP. Ultrasound induced cavitation and sonochemical yield. *J Acoust Soc Am* 1998;104:2675–2682.
21. Sochard S, Wilhelm AM, Delmas H. Modeling of free radicals production in a collapsing gas-vapor bubble. *Ultrason Sonochem* 1997;4:77–84.
22. Moss WC, Yound DA, Harte JA, Levalin JL, Rozsnyai BF, Zimmerman GB, Zimmerman JH. Computed optical emissions from sonoluminescing bubbles. *Phys Rev E* 1999;59:2986–2992.
23. Yasui K. Alternative model for single bubble sonoluminescence. *Phys Rev E* 1997;56:6750–6760.
24. Yasui K. Chemical reactions in a sonoluminescing bubble. *J Phys Soc Jpn* 1997;66:2911–2920.
25. Storey BD, Szeri AJ. Water vapor, sonoluminescence and sonochemistry. *Proc R Soc Lond A* 2000;456:1685–1709.
26. Colussi AJ, Weavers LK, Hoffmann MR. Chemical bubble dynamics and quantitative sonochemistry. *J Phys Chem A* 1998;102:6927–6934.
27. Colussi AJ, Hoffmann MR. Vapor supersaturation in collapsing bubbles: relevance to mechanisms of sonochemistry and sonoluminescence. *J Phys Chem A* 1999;103:11336–11339.
28. Toegel R, Gompf B, Pecha R, Lohse D. Does water vapor prevent upscaling sonoluminescence. *Phys Rev Lett* 2000;85:3165–3168.
29. Kwak HY, Yang H. An aspect of sonoluminescence from hydrodynamic theory. *J Phys Soc Jpn* 1995;64:1980–1992.
30. Kwak HY, Na JH. Physical processes for single bubble sonoluminescence. *J Phys Soc Jpn* 1997;66:3074–3083.

31. Kwak HY, Na JH. Hyrodynamic solutions for sonoluminescing gas bubble. *Phys Rev Lett* 1996;77:4454–4457.
32. Fujikawa S, Akamatsu T. Effect of the non-equilibrium condensation of vapor on the pressure wave produced by the collapse of a bubble in liquid. *J Fluid Mech* 1980;97:481–512.
33. Brennen CE. *Cavitation and Bubble Dynamics*. Oxford: Oxford University Press, 1995.
34. Prosperetti A, Lezzi A. Bubble dynamics in a compressible liquid, Part 1: First order theory. *J Fluid Mech* 1986;168:457–477.
35. Hsieh DY, Plesset MS. Theory of rectified diffusion of mass into gas bubbles. *J Acoust Soc Am* 1961;33:206–215.
36. Eller AI, Flynn HG. Rectified diffusion through non-linear pulsations of cavitation bubbles. *J Acoust Soc Am* 1965;37:493–503.
37. Safar MH. Comments on the paper concerning rectified diffusion of cavitation bubbles. *J Acoust Soc Am* 1968;43:1188–1189.
38. Lofstedt R, Weninger K, Puttermann SJ, Barber BP. Sonoluminescing bubbles and mass diffusion. *Phys Rev E* 1995;51:4400–4410.
39. Fyrillas M, Szeri AJ. Dissolution and growth of soluble spherical oscillating bubbles. *J Fluid Mech* 1994;277:381–407.
40. Crank J. *The Mathematics of Diffusion*. Oxford: Clarendon Press, 1975.
41. Hirschfelder JO, Curtiss CF, Bird RB. *Molecular Theory of Gases and Liquids*. New York: Wiley, 1954.
42. Condon EU, Odishaw H. *Handbook of Physics*. New York: McGraw Hill, 1958.
43. Reid RC, Prausnitz JM, Poling BE. *Properties of Gases and Liquids*. New York: McGraw Hill, 1987.
44. Horvath AL. *A Handbook of Aqueous Electrolyte Solutions*. Chichester: Ellis Horwood, 1985.
45. Press WH, Teukolsky SA, Flannery BP, Vetterling WT. *Numerical Recipes*. New York: Cambridge University Press, 1992.
46. Prosperetti A, Commander KW. Linear pressure waves in bubbly liquids: comparison between theory and experiments. *J Acoust Soc Am* 1989;85:732–746.
47. Sangeeth Krishnan J, Dwivedi P, Moholkar VS. Numerical investigation into the chemistry induced by hydrodynamic cavitation. *Ind Eng Chem Res* 2006;45:1493–1504.
48. Eriksson G. Thermodynamic studies of high temperature equilibria. XII. SOLGASMIX, a computer program for calculation of equilibrium composition in multiphase system. *Chem Scr* 1975;8:100–103.
49. Hart EJ, Henglein A. Free radical and free atom reactions in the sonolysis of aqueous iodide and formate solutions. *J Phys Chem* 1985;89:4342–4347.

Appendix: Calculation of the Acoustic Pressure Amplitude

The pressure amplitude of the acoustic wave produced by the ultrasound probe was determined by calibrating the ultrasonic processor using calorimetric method. This method is based on the assumption that all of the energy delivered to the reaction medium is dissipated as heat.

During the sonication of the degassed as well as saturated reaction medium for 10 min, the temperature of the medium (150 ml of KI solution) increased by 1°C with theoretical maximum power input of 100 W. This would mean that the actual rate of energy input to the system (ignoring minor changes in heat capacity of water with dissolution of KI) was:

$$\frac{mc_p\Delta T}{t} = \frac{0.15 \times 4180 \times 1}{600}\frac{\text{Joule}}{\text{seconds}} = 1.045 \text{ W}.$$

The tip of ultrasound horn had a diameter of 13 mm, and thus, the acoustic intensity is calculated as:

$$I = \frac{\text{Actual power (W)}}{\text{Area of horn tip (m}^2\text{)}} = \frac{1.045}{\frac{\pi}{4}(13 \times 10^{-3})^2} = 7873 \text{ W/m}^2.$$

The relation between acoustic intensity and acoustic pressure amplitude is given as: $I = \frac{P_A^2}{2\rho c}$, where ρ is the density of the medium and c is the speed of sound in the medium. Again, ignoring minor changes to these parameters for water with dissolution of KI, we substitute $\rho = 1000$ kg/m^3 and $c = 1481$ m/s. The acoustic pressure amplitude is then calculated as:

$$P_A = \sqrt{2I\rho c} = \sqrt{2 \times 7873 \times 1481 \times 1000} = 1.527 \times 10^5 \text{ Pa} = 1.527 \text{ bar} \approx 1.5 \text{ bar}.$$

Manuscript received Sept. 13, 2006, and revision received Feb. 26, 2007.